Chapter 7

The time-dependence of the cosmic ray transport coefficients

7.1 Introduction

In the previous chapter it was shown that the numerical model, which incorporated new theoretical advances (*Teufel and Schlickeiser*, 2002, 2003; *Shalchi et al.*, 2004; *Minnie et al.*, 2007) in the transport coefficients, computed cosmic ray intensities along the Voyager 1 trajectory and at Earth which are compatible to observations on a global scale. However, after ∼2004 the model failed to reproduce the observations at Earth even after changing various different parameters like the heliopause position, TS position, shock compression ratio and diffusion coefficients.

As shown in the previous chapter the diffusion coefficients had a particular dependence on δB^2 and B (as given by Equations 6.5 and 6.10) which change over a solar cycle (as shown in Figure 6.3). Also it was assumed that the drift coefficient changes over a solar cycle, as given by Equation 6.12 and shown in Figure 6.1. For this coefficient the current sheet tilt angle α was assumed as a proxy for solar activity. In this chapter, the time-dependence in the different transport coefficients arising from the assumptions of δB^2, B and α, and the effect on cosmic ray intensities will be investigated.

7.2 Effect of different variance

From Equations 6.5 and 6.10, it follows that the diffusion coefficients have a particular dependence on the variance δB^2. In Figure 7.1, the statistical variance calculated from magnetic field measurements are shown as the dashed blue line. This δB^2 is used in the model and transported with the solar wind from the inner boundary radially outward. Shown in Figure 7.1 is how δB^2 changes over a solar cycle, see also *Smith et al.* (2006b). To investigate the effect of a possible different amplitude in δB^2 between solar minimum and maximum on cosmic ray modulation, the amplitude is first increased. This is done by manipulating the calculated variance by assuming $\left(\delta B^2\right)^{1.5}$ instead of δB^2 in the model in order to change the amplitude. Note

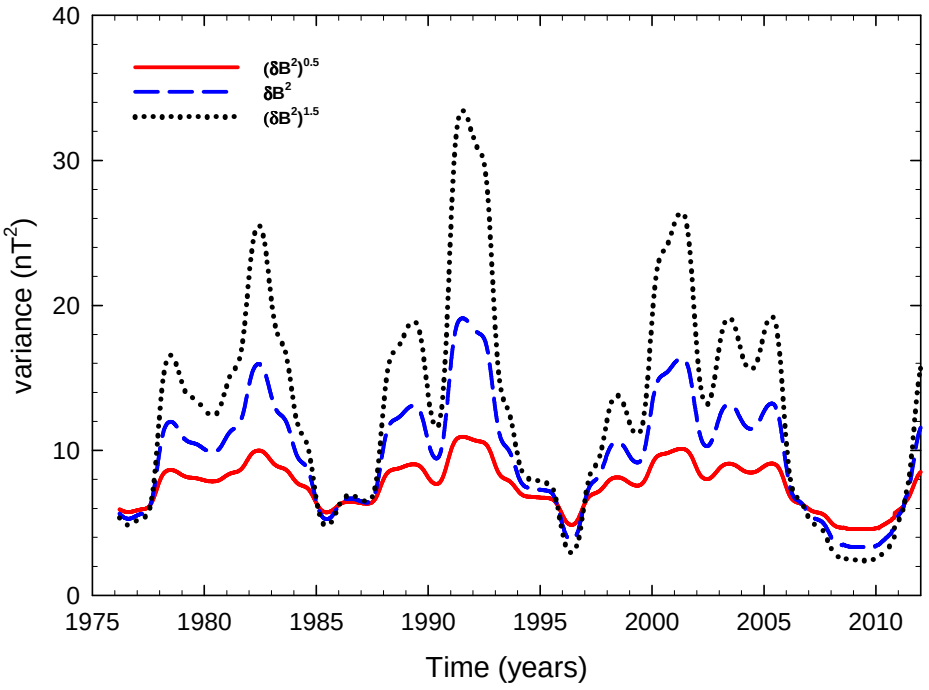

Figure 7.1: Shown are the smoothed yearly variance δB^2 (dashed line), a scaled up δB^2 (dotted line) and a scaled down δB^2 (solid line).

that values are normalised to original δB^2 values at solar minimum (i.e. 5 nT^2). The amplitude between solar minimum and maximum can also be decreased by assuming $\left(\delta B^2\right)^{0.5}$ instead of δB^2 in the model, and again normalise at solar minimum. Note that these manipulations of δB^2 are done only to change the amplitude between solar minimum and maximum and does not imply that the diffusion coefficients depend differently on the variance as given by Equations 6.4 and 6.9 for $\lambda_{||}$ and $\lambda_{\perp}$ respectively.

The corresponding three scenarios are shown in Figure 7.1 and computed cosmic ray results are shown in Figure 7.2. As reported in the previous chapter, the calculated statistical variance δB^2 computes globally compatible result along the Voyager 1 trajectory and at Earth (except $\sim$2004 onwards). However, shown in Figure 7.2 is that the $\left(\delta B^2\right)^{0.5}$ scenario produced a better result compared to the δB^2 scenario, especially for solar maximum periods. This may suggest that a variance with smaller amplitude between solar maximum and minimum is better suited as input parameter for an optimal modelled result. Also found is that the variance does not have a profound effect for solar minimum compared to other parameters. However, during solar maximum periods and along the Voyager 1 trajectory, the way the variance is scaled has a more pronounced effect on the computed intensities. Even after varying the variance, the model failed to reproduce a compatible result at Earth after $\sim$2004 when compared to observations.

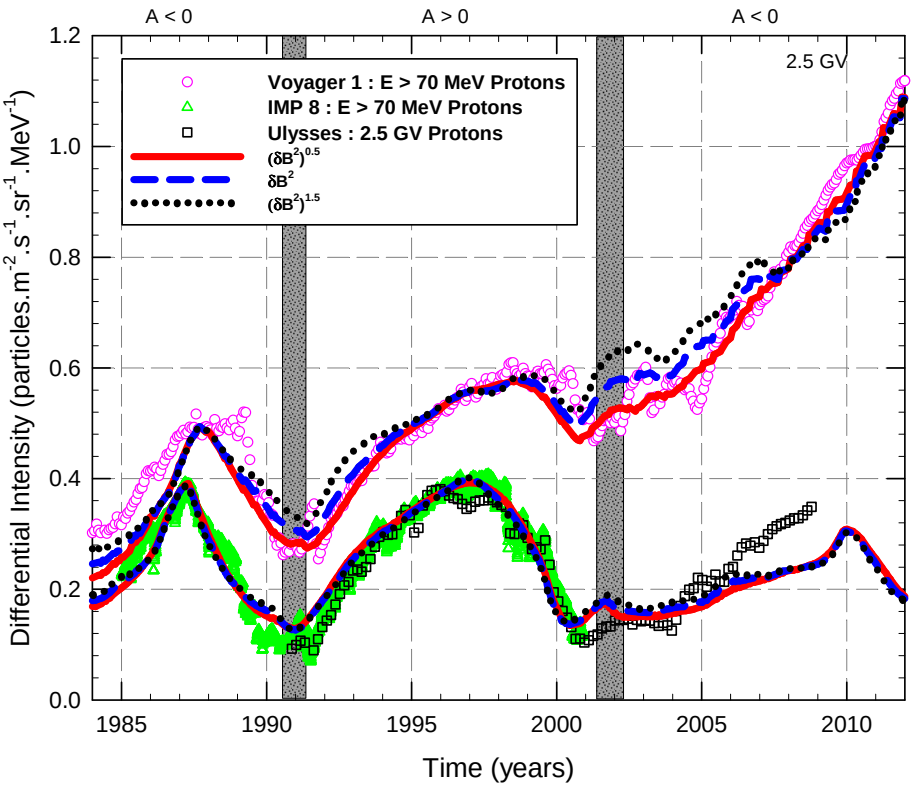

Figure 7.2: Computed 2.5 GV cosmic ray proton intensities at Earth and along the Voyager 1 trajectory since 1984 are shown for differently scaled variance as a function of time. Also shown are the $E > 70$ MeV proton observations from Voyager 1 (from http://voyager.gsfc.nasa.gov) as symbols (circles) and $E > 70$ MeV measurements at Earth from IMP 8 (from http://astro.nmsu.edu) (triangles) and ~ 2.5 GV proton observations (squares) from Ulysses (*Heber et al.*, 2009). The shaded areas represent the periods where there was not a well defined HMF polarity.

7.3 Effect of different K_{A0} values

Figure 7.3 shows computed results corresponding to different K_{A0} values as given in Equation 6.12. This constant scales the drift coefficient. In this figure, four different scenarios are shown where $K_{A0} = 1.0$ represents a full drift scenario and $K_{A0} = 0.0$ represents a no drift scenario. Note that all coefficients still change over a solar cycle via Equations 6.11, 6.5 and 6.10 respectively. For extreme solar maximum periods, K_A is almost zero via Equation 6.11 resulting in nearly the same solutions for all K_{A0} values for this level of solar activity. The $K_{A0} = 1.0$ scenario gives maximum drift effects for solar minimum, which in-turn leads to a maximum cosmic ray intensities during solar minimum periods. When K_{A0} is decreased from 1.0 to 0.8, to 0.6 and finally to 0.0, the cosmic ray intensities are also decreasing during solar minimum. Note that $K_{A0} = 0.8$ is considered as an optimal model result when comparing to the observations along the Voyager 1 trajectory and at Earth until ~2004. Again after 2004, the model disagrees with the observations at Earth even for a maximum drift scenario $K_{A0} = 1.0$.

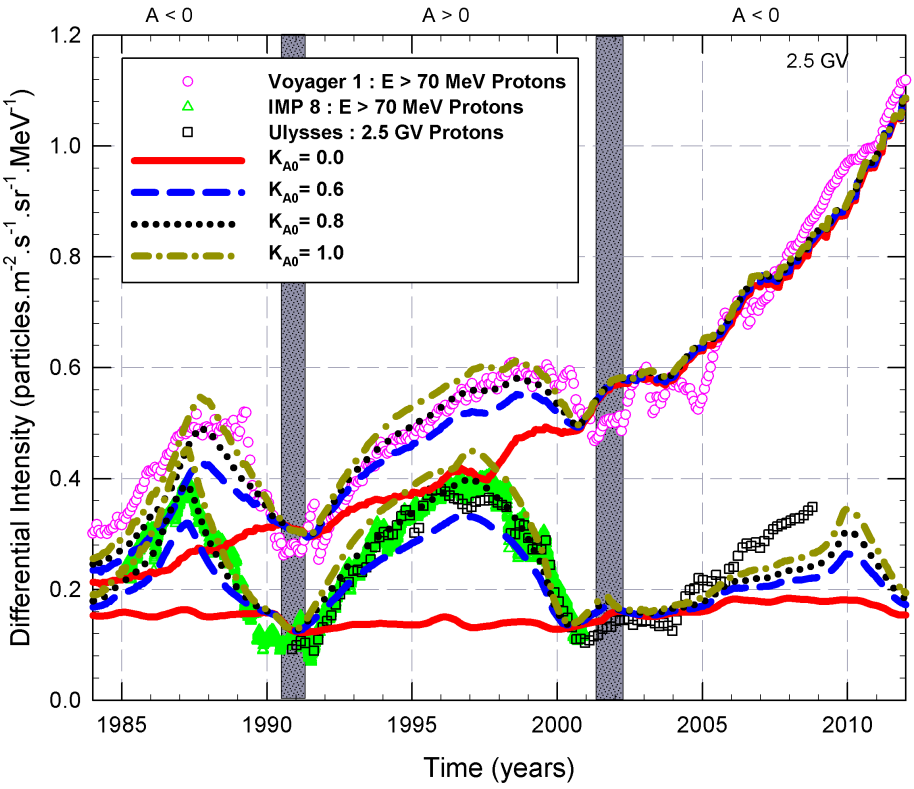

Figure 7.3: Similar to Figure 7.2 except that here computed results at Earth and along the Voyager 1 trajectory are shown for different K_{A0} values, representing different drift coefficeint values.

From this figure, it follows that the amplitude between solar minimum and solar maximum are largely dependent on the magnitude of the drift coefficient. The $K_{A0} = 0.8$ assumption results in compatible intensities, and when this coefficient is reduced the computed amplitude between solar minimum and maximum is decreasing. This suggests that in the model, the computed time-dependence is dominated by solar-cycle related changes in the drift coefficient (*Ndiitwani*, 2005; *Visser*, 2010), as shown in Figure 7.3 where the solid red line (zero drift) shows almost no variation over a solar cycle. However, as will be shown below, the failure of the model to reproduce compatible cosmic ray intensities at Earth when compared to observations after ∼2004 indicates that the assumption of the time-dependence in the transport parameters as given by Equations 6.11, 6.5 and 6.10 is not optimal. This aspect is discussed next.

7.4 Modifying time-dependence

After a thorough parameter study, it is found that when δB^2 and B (as shown in Figure 6.2) are used as time-varying input parameters, the model successfully computed cosmic ray observation along the Voyager 1 trajectory and at Earth until ∼2004, but failed to reproduce cosmic ray modulation at Earth after ∼2004. It is also shown that the cosmic ray modulation over a solar

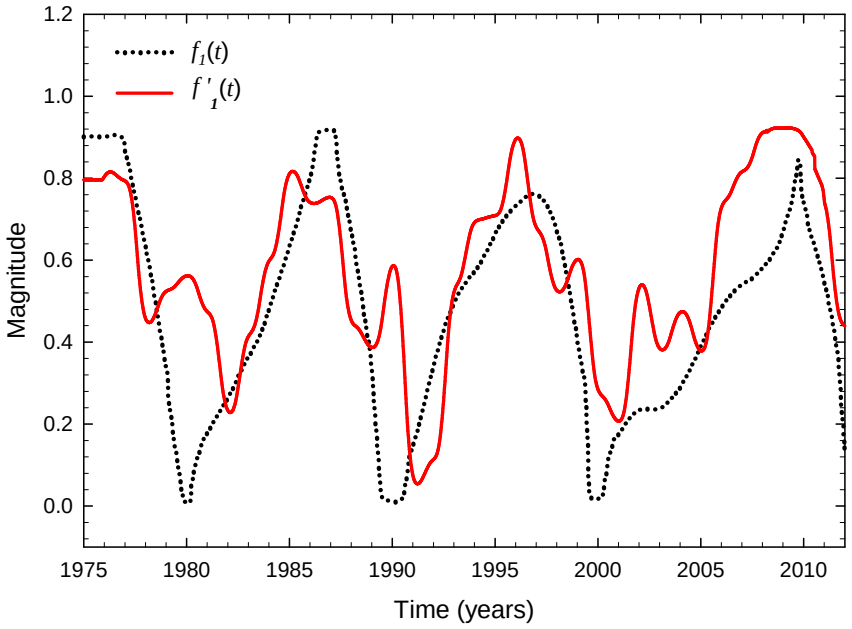

Figure 7.4: Shown are the time-dependent drift function $f_1(t)$ and the modified time-dependent drift function $f_1'(t)$.

cycle computed using these parameters is dominated by time-dependent changes in the drift coefficient. In a first attempt to compute compatibility with observations at Earth after ∼2004, the time-dependence in the drift coefficient is modified by constructing a new time-dependent function.

7.4.1 Modifying $f_1(t)$, the time-dependence in the drift coefficient

As shown before, the model failed to reproduce the observed cosmic ray modulation at Earth from ∼2004 onwards, so a modified time-dependent function $f_1'(t)$ for drifts is tested and the results are compared with the observations for this period. To construct a different time-dependent function, the comparison between the model and observations at Earth after ∼2004 is used as a guide. From this, it follows that the observed intensities are increasing faster compared to the model results as a function of decreasing solar activity. A function is therefore needed which recovers drift effects earlier compared to the current function as solar activity is decreasing. The time-dependence in the drift coefficient $f_1(t)$ as given in Equation 6.11 is now modified. Note that $f_1(t)$ uses the tilt angle as the only input parameter but for the modified function the variance δB^2 is used (*Minnie et al.*, 2007). Different expressions were examined with an optimal expression for $f_1'(t)$ given as,

$$f_1'(t) = 1.106 - \frac{0.055\delta B^2(t)}{{\delta B_o}^2}, \tag{7.1}$$

with ${\delta B_o}^2 = 1$ nT^2.

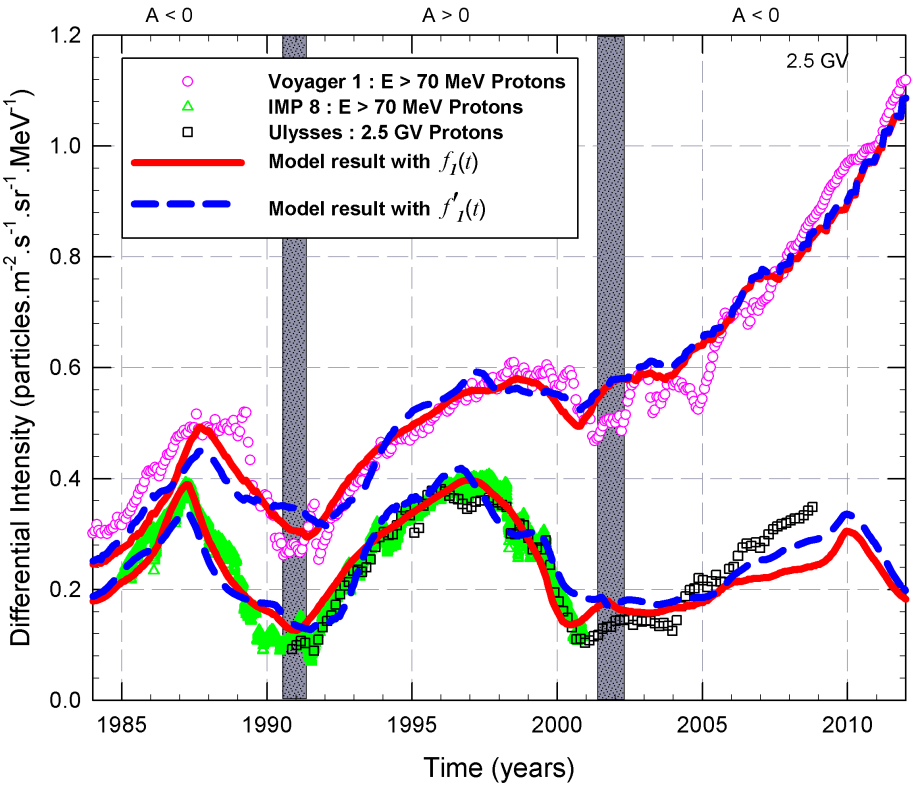

Figure 7.5: Similar to Figure 7.2 except that here model results at Earth and along the Voyager 1 trajectory are shown for $f_1(t)$ and $f'_1(t)$.

A comparison between the previous time-dependent function $f_1(t)$ and the function $f'_1(t)$ is shown in Figure 7.4. The figure shows that there is a phase-difference between $f'_1(t)$ and $f_1(t)$ due to their dependence on different parameters. However, more important is that for the period from ∼2004 onwards, the new function $f'_1(t)$ is increasing much faster compared to $f_1(t)$ as a function of decreasing activity. As a matter of fact, this function recovers drifts almost immediately to full drifts after ∼2004 and should compute more realistic cosmic ray intensities after ∼2004 if the time-dependence in this coefficient dominates the recovery of intensities to solar minimum values.

Figure 7.5 shows the computed cosmic ray intensities assuming $f_1(t)$ and $f'_1(t)$ in the model. Shown is that overall $f_1(t)$ computed a better compatible result when compared to the modified function $f'_1(t)$. However, for the period from ∼2004 onwards at Earth, the new function calculated higher intensities than the previous function but still the calculated intensities are much lower than the observations and the desired recovery of cosmic ray intensities toward solar minimum is not achieved. In the next section it will be shown that a modification also in the time-dependence of the diffusion coefficients (as given by $f_2(t)$ and $f_3(t)$) is needed which is discussed next.

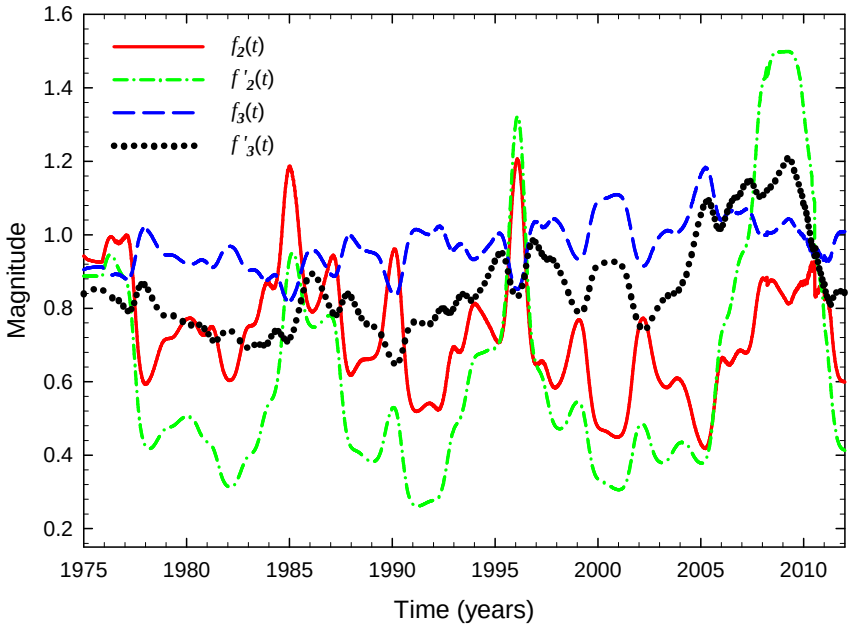

Figure 7.6: Shown are the parallel and perpendicular time-dependent functions $f_2(t)$ and $f_3(t)$ compared to the modified parallel and perpendicular time-dependent functions $f_2'(t)$ and $f_3'(t)$.

7.4.2 Modifying $f_2(t)$ and $f_3(t)$, the time-dependence in diffusion

In the previous section, the time-dependence in the drift coefficient was investigated to see whether modifications in this coefficient could lead to a better compatibility between model and observations after ∼2004 at Earth. In this section, the time-dependence in diffusion coefficients are modified by inspecting Equations 6.3 and 6.8, as given by *Teufel and Schlickeiser* (2003) and *Shalchi et al.* (2004). Instead of arbitrarily choosing a different time-dependence or phenomenologically constructing one by comparing model results with observations, the time-dependence in Equations 6.3 and 6.8 which are applicable to higher rigidities, e.g. $\gtrsim 4$ GV, are used here at 2.5 GV. Note that due to the rigidity dependence of different terms (which depend differently on δB^2 and B) in the expressions of $\lambda_{||}$ and $\lambda_{\perp}$, there is a time-dependence in the rigidity dependence.

Note that for high rigidities, e.g. $\gtrsim 4$ GV, the term $\left[\frac{b_k}{4\sqrt{\pi}} + \frac{2}{\sqrt{\pi}(2-s)(4-s)}\frac{b_k}{R^s}\right]$ in Equation 6.3 can be approximated to be a constant C and one can write

$$\lambda_{||} = \frac{3s}{\sqrt{\pi}(s-1)} \frac{R^2}{b_k\, k_{min}} \left(\frac{B}{\delta B_{slab,x}}\right)^2 C, \tag{7.2}$$

which results in a time-dependence for $\lambda_{||}$ as,

$$\lambda_{||} \propto \left(\frac{1}{\delta B_{slab,x}}\right)^2. \tag{7.3}$$

See also *Manuel et al.* (2011a,c). Note that B in Equation 7.2 is cancelled by the B in the R_L (see

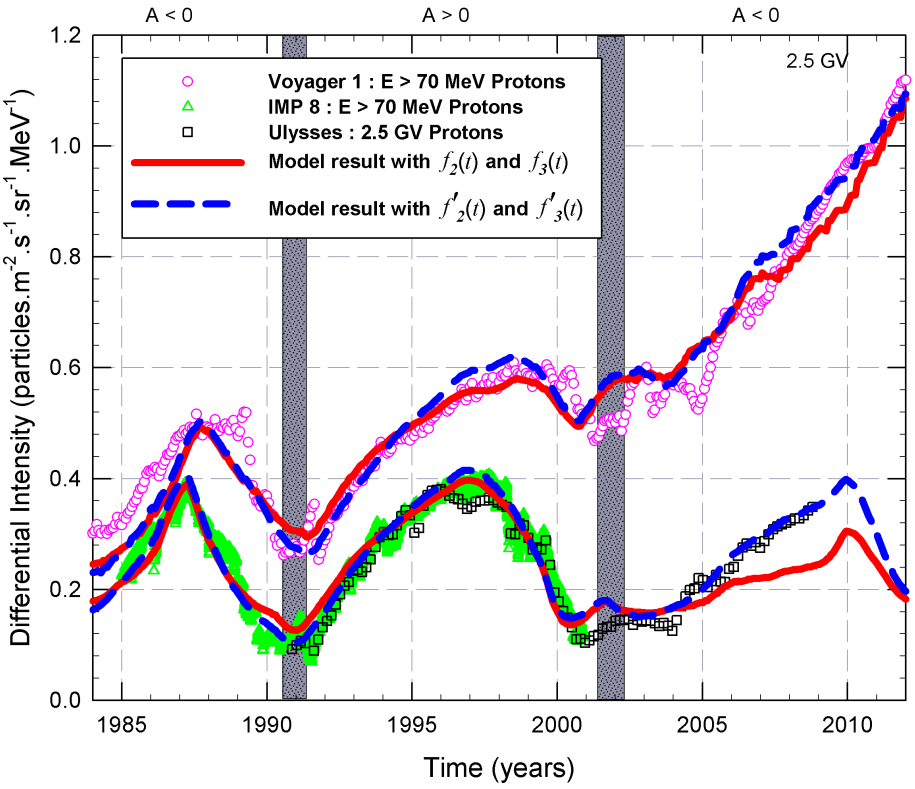

Figure 7.7: Similar to Figure 7.2 except that here model results at Earth and along the Voyager 1 trajectory are shown for time-dependent functions $f_2(t)$ and $f_3(t)$ and the modified time-dependent functions $f'_2(t)$ and $f'_3(t)$.

Section 6.2.1) to give Equation 7.3, from which the function $f'_2(t)$, can be written as,

$$f'_2(t) = C_4 \left(\frac{1}{\delta B(t)} \right)^2 , \tag{7.4}$$

with C_4 a constant in units of (nT)^2.

For the perpendicular diffusion coefficient it can also be assumed for $P \gtrsim 4$ GV that,

$$\lambda_\perp \propto \left(\frac{\delta B_{2D}}{B} \right)^{\frac{4}{3}} \left(\frac{1}{\delta B_{slab,x}} \right)^{\frac{2}{3}} . \tag{7.5}$$

From Equation 7.5 the modified time-dependence for the perpendicular diffusion coefficient, which is described by the function $f'_3(t)$, can be deduced as,

$$f'_3(t) = C_5 \left(\frac{\delta B(t)}{B(t)} \right)^{\frac{4}{3}} \left(\frac{1}{\delta B(t)} \right)^{\frac{2}{3}} , \tag{7.6}$$

with C_5 a constant in units of (nT)$^{2/3}$.

A comparison between the previous $f_2(t)$ and new $f'_2(t)$ (time-dependence in parallel diffusion coefficient) and the previous $f_3(t)$ and new $f'_3(t)$ (time-dependence in perpendicular diffusion coefficient) is shown in Figure 7.6. The new $f'_2(t)$ and $f'_3(t)$ shows a larger difference between

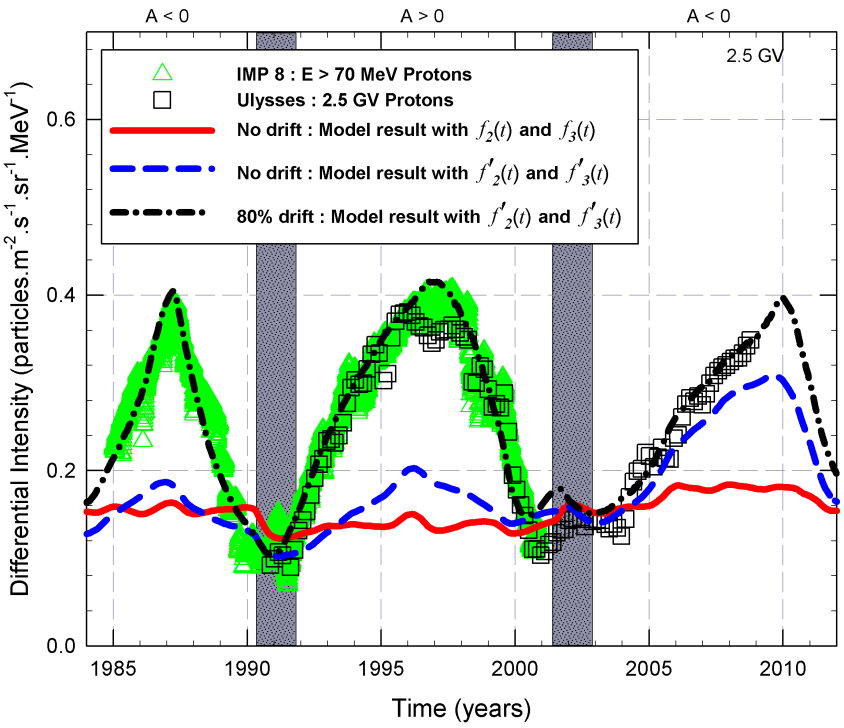

Figure 7.8: Computed 2.5 GV cosmic ray proton intensities at Earth since 1984 are shown for two no drift scenarios assuming recent theory time-dependences ($f_2(t)$ and $f_3(t)$) and modified recent theory time-dependences ($f'_2(t)$ and $f'_3(t)$). A third scenario with the modified recent theory time-dependence with 80% drift fitting the cosmic ray proton observations at 1 AU is also shown. Also shown are the proton observations from $\sim$ 2.5 GV proton observations from Ulysses (squares) (*Heber et al.*, 2009) and $E > 70$ MeV measurements from IMP 8 (triangles) (from `http://astro.nmsu.edu`).

solar minimum and solar maximum when compared to the previous $f_2(t)$ and $f_3(t)$. This modified time-dependence is closer to the traditional compound approach as constructed by *Ferreira and Potgieter* (2004) where the time-dependence in all the transport coefficients change roughly by a factor of $\sim$10 between solar minimum and maximum.

Model results using $f'_2(t)$ and $f'_3(t)$ are now compared to results from $f_2(t)$ and $f_3(t)$ and is shown in Figure 7.7. It is shown that there is no significant differences between the different scenarios apart after $\sim$2004 at Earth. As shown, the introduction of $f'_2(t)$ and $f'_3(t)$ in the model resulted in a better compatibility between the observations and the model after $\sim$2004 at Earth. Therefore, for this particular polarity cycle the amplitude between solar minimum and maximum in the different diffusion coefficients as given by $f_2(t)$ and $f_3(t)$ is too small and a larger amplitude is necessary to compute realistic modulation, as given by $f'_2(t)$ and $f'_3(t)$.

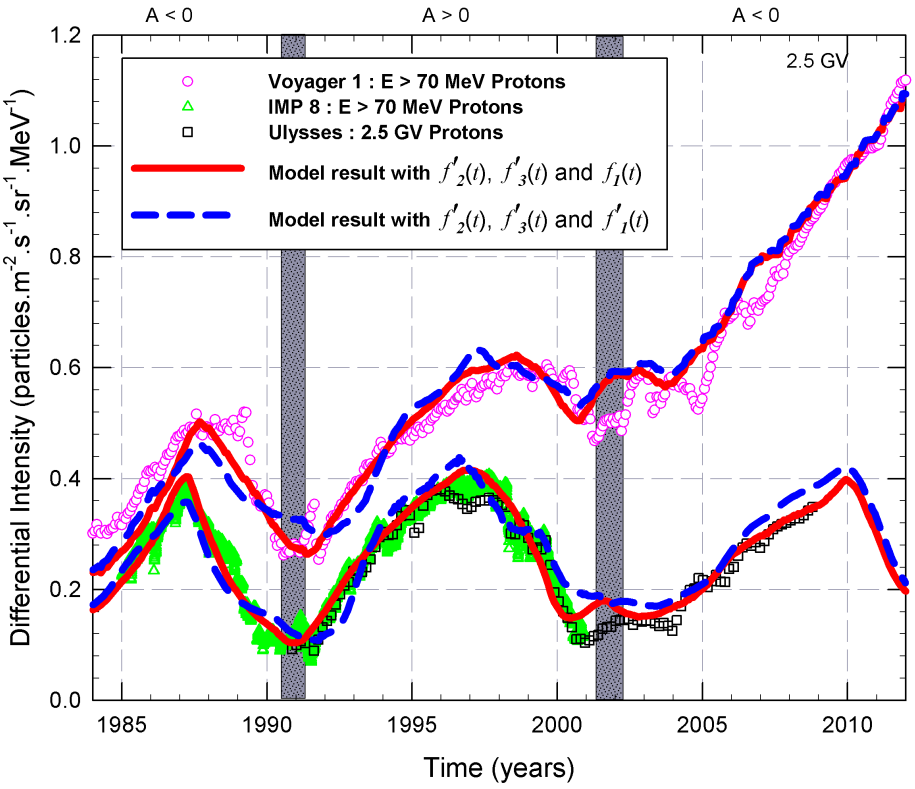

Figure 7.9: Similar to Figure 7.2 except that here model results at Earth and along the Voyager 1 trajectory are shown for $f_1(t)$ and $f'_1(t)$ while using time-dependent functions $f'_2(t)$ and $f'_3(t)$.

7.4.3 The effect of a modified time-dependence of $f'_2(t)$ and $f'_3(t)$ on model computations

The model results using the time-dependent functions, $f_2(t)$ and $f_3(t)$, result in computations where changes in the cosmic ray intensities can be directly correlated to time-dependent changes in the magnitude of the drift coefficient. In this chapter this aspect is revisited and modifications $f'_2(t)$ and $f'_3(t)$ were proposed and the result was shown in Figure 7.7.

In Figure 7.8, the no drift scenarios of $f_2(t)$ and $f_3(t)$ are compared to the modified $f'_2(t)$ and $f'_3(t)$, and two scenarios, namely the no drift scenario and $K_{A0} = 0.8$ scenario is shown at Earth from 1984 onwards. In comparison the ∼2.5 GV Ulysses and $E > 70$ MeV IMP 8 observations are shown. From this figure it follows that the no drift $f'_2(t)$ and $f'_3(t)$ scenario result in a computed amplitude between solar minimum and maximum which is much larger, especially after ∼2004 onwards compared to the previous assumptions. The modified $f'_2(t)$ and $f'_3(t)$ with $K_{A0} = 0.8$ computed a compatible result at Earth from ∼2004 onwards, showing that a larger time-dependence in the magnitude of the diffusion coefficients are needed over this solar cycle. The modified $f'_2(t)$ and $f'_3(t)$ indicate that, for this particular solar cycle at Earth, time-dependent changes in the diffusion coefficients are more important compared to previous cycles. This can be seen by first comparing the dashed blue line with the solid red line showing

a much larger modulation amplitude, and then comparing the dashed-dotted black line, to previous attempts as in the previous chapter. For this particular solar cycle, the drift effects are downplayed by changes in the diffusion coefficients. This aspect of the recent solar minimum period was also discussed in detail by *Vos* (2012) and *Potgieter et al.* (2012).

Because the modified $f_2'(t)$ and $f_3'(t)$ result in compatible modulation at Earth from ∼2004 onwards and not really influencing results elsewhere as shown in Figure 7.7, these modified expressions are now used further in the model (*Manuel et al.*, 2011a,c). However, in the previous section a modification in the time-dependence of the drift coefficient $f_1(t)$ were proposed namely, $f_1'(t)$. This modification was an attempt to fit observations at Earth better for the period ∼2004 onwards. Figure 7.9 shows model results assuming $f_1(t)$ and $f_1'(t)$ respectively. Both the functions successfully reproduced the cosmic ray modulation in the heliosphere on a global scale. The new function $f_1'(t)$ which uses δB^2 as the input parameter for the time-dependence in drift computed better results than $f_1(t)$ for the ∼1997–2001 period where $f_1(t)$ calculated lower intensities than the observations. But $f_1'(t)$ computed higher intensities than observations and failed to reproduce observations during solar maximum periods and for the periods ∼1995–1997 and ∼2006–2010. Also $f_1'(t)$ result computed lower intensities than observations for the period ∼1987–1989. However, on a global scale the computed model result by $f_1(t)$ when compared to $f_1'(t)$ produced better compatibility with the observations. From this point on for the model computations the time-dependence in drift is considered to be $f_1(t)$, which uses tilt angle as input parameter as proposed by *Ndiitwani* (2005).

7.5 A comparison between the previous compound approach and the modified approach

The compound approach (see discussion in Chapter 5) was introduced by *Ferreira* (2002), *Ferreira and Potgieter* (2004) and is based on an empirical approach where modelled results are compared to observations in order to construct a realistic time-dependence in the transport coefficients. This was done because of a lack of a clear theory on how the diffusion and drift coefficients should change over a solar cycle. However, recent progress by *Teufel and Schlickeiser* (2002, 2003), *Shalchi et al.* (2004), *Minnie et al.* (2007) and *Engelbrecht* (2008) gives a much clearer picture of how the diffusion coefficients depend on basic turbulence quantities, such as the magnetic field magnitude and variance, which change over a solar cycle. A modified compound approach $f_2'(t)$ and $f_3'(t)$ is developed from these recent theoretical developments as discussed above.

Here a comparison between the successfully tested compound approach to the modified compound approach used in this work is discussed. Figure 7.10 shows that at Earth and along the Voyager 1 trajectory, the modified approach resulted in a better model result than the compound approach on a global scale. The original compound approach successfully calculated cosmic ray intensity along the Voyager 1 trajectory for a period ∼2000–2003 when modified

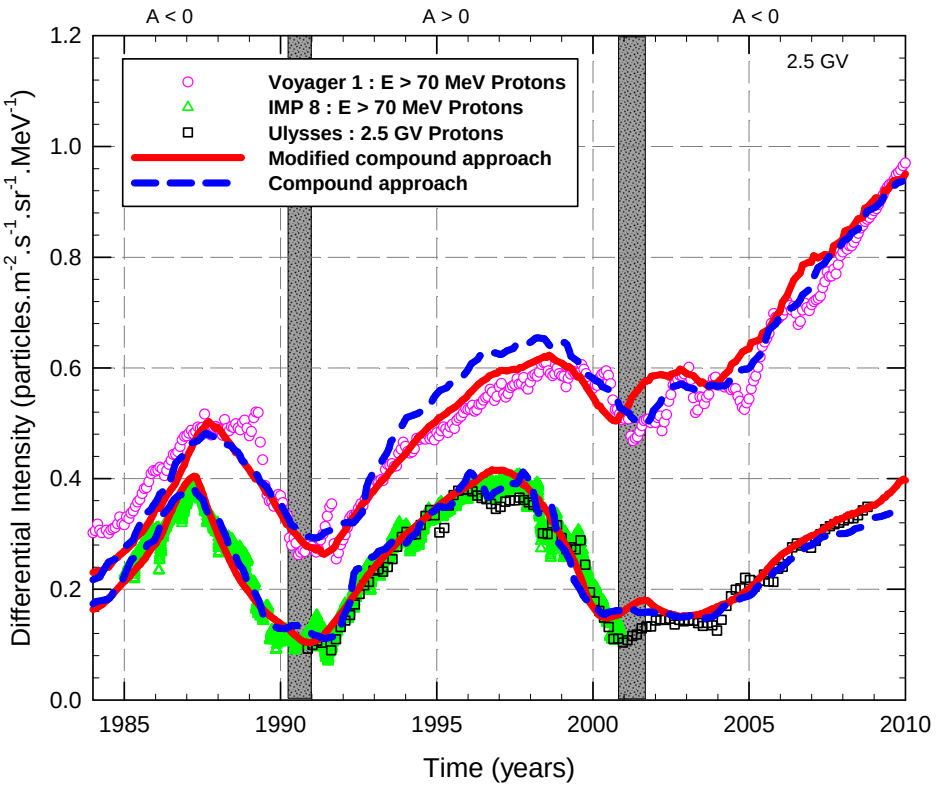

Figure 7.10: Similar to Figure 7.2 except that here model results at Earth and along the Voyager 1 trajectory are shown for the previous compound approach and the modified compound approach.

approach failed to reproduce these observations. For the period ∼1993–1999 the compound approach calculated higher intensities than the observations but for this period the modified approach successfully reproduced the observations along the Voyager 1 trajectory. Both approaches failed to reproduce the step increase/decrease in cosmic ray intensities in the spacecraft measurements. Overall, the modified approach which uses recent theories compares well to the previous compound approach to compute global cosmic ray modulation in the heliosphere.

7.6 Summary and conclusions

In the previous chapter it was shown that after incorporating recent theoretical advances in the transport coefficients by *Teufel and Schlickeiser* (2002, 2003), *Shalchi et al.* (2004), *Minnie et al.* (2007) and *Engelbrecht* (2008), the time-dependence resulting from these expressions failed to reproduce observations at Earth after ∼2004 when δB^2, B and α were used as input parameters. This suggested a possible modification to the time-dependence. This chapter studied this by firstly investigating the effect of the time-dependence in δB^2 on the cosmic ray modulation. It was found that a smaller amplitude in the variance from solar minimum to maximum is

more appropriate compared to the calculation of statistical variance as done in this work and shown in Figure 6.2. However, this still failed to reproduce the observations at Earth from ∼2004.

The effect of the drift coefficient on the cosmic ray modulation was investigated and it was found that the time-dependence, resulted from the above mentioned theoretical advances is mostly due to changes in the drift coefficient over a solar cycle. A modification to the time-dependent function $f_1(t)$, which scales drifts over a solar cycle, was proposed. Although this modified function recovers drift effects faster towards solar minimum, it was not sufficient to compute compatible results after ∼2004.

The time-dependence in parallel and perpendicular diffusion coefficients, $f_2(t)$ and $f_3(t)$ respectively, was modified by introducing a new time-dependence, $f_2'(t)$ and $f_3'(t)$ given by Equations 7.4 and 7.6. This leads to a compatible model result along the Voyager 1 trajectory and at Earth even for the period after ∼2004. Assuming this, cosmic ray modulation especially for this polarity cycle is no longer largely determined by changes in the drift coefficient but also changes in the diffusion coefficients over time contribute to long-term cosmic ray modulation.

This newly modified $f_2'(t)$ and $f_3'(t)$ computed results which compared well with the traditional compound approach of *Ferreira* (2002), *Ferreira and Potgieter* (2004) and the observations along the Voyager 1 and at Earth on a global scale. However, for extreme solar maximum conditions the computed step-like modulation is not as pronounced as observed, indicating that some merging in the form of global interaction regions is needed.